Planar equilibria of sessile and pendant liquid drops on geometrically non-linear elastic membranes

Vineet Nair, Ishan Sharma, and V. Shankar

Citation: Physics of Fluids **30**, 082114 (2018); doi: 10.1063/1.5046155
View online: https://doi.org/10.1063/1.5046155
View Table of Contents: http://aip.scitation.org/toc/phf/30/8
Published by the American Institute of Physics

Planar equilibria of sessile and pendant liquid drops on geometrically non-linear elastic membranes

Vineet Nair,[1,a)] Ishan Sharma,[1] and V. Shankar[2]
[1]*Mechanics and Applied Mathematics Group, Department of Mechanical Engineering, Indian Institute of Technology Kanpur, Kanpur 208016, India*
[2]*Department of Chemical Engineering, Indian Institute of Technology Kanpur, Kanpur 208016, India*

(Received 26 June 2018; accepted 8 August 2018; published online 29 August 2018)

Equilibrium shapes are obtained for sessile and pendant liquid drops placed on elastic membranes in two-dimensions. The membrane is allowed to undergo large deformations under the action of capillary forces and fluid pressure. We focus on the global characteristics of the system, like the equilibrium shape of the drop, the membrane's deformed shape, the apparent contact angle and contact size, and their variation with the volume of the drop for different membrane tensions and drop apex curvatures. It is found that the apparent contact angle is not simply a function of material property but of the system's geometry as well. The contact size for sessile drops shows a non-monotonic behavior with the volume for all drop apex curvatures. However, for pendant drops, the behavior is strictly monotonic below a critical value of the drop apex curvature. *Published by AIP Publishing.*
https://doi.org/10.1063/1.5046155

I. INTRODUCTION

Elastocapillarity is the study of interactions between capillary forces and elastic forces.[1–5] It has long been known that a liquid drop placed on a soft substrate deforms it.[6–18] With increasing interest and focus on areas such as micro- and nano-scale technologies, bioengineering, and flexible electronics, there has been a renewed interest in this area by way of experiments[19–28] and modeling.[21,29–36] The interaction between capillarity and elasticity has been employed to increase the density of nucleation of water drops,[37] modify the adhesive behavior of soft gels,[38,39] understand pattern formation using droplet migration,[40] study the interaction between droplets in view of coalescence and coarsening,[41] understand wrinkling[42–44] and capillary origami,[45–48] control the droplet's splash upon impact,[49] measure bulk stresses in soft solids,[50] and measure surface stresses in soft solids[23,24,51] and, more recently, strain-dependent surface stresses.[27,28,52,53] Recent studies reveal that solid surface stresses may also play an important role at larger length scales.[27]

Das *et al.*[54] used density functional theory to compute capillary forces exerted by a sessile drop resting on a solid substrate. They report that besides the normal component of the force, there exists a tangential component near the contact line. Marchand *et al.*[55] used density functional theory to determine contact angle selection and reported that the contact angle is selected at a microscopic scale. Lubbers *et al.*[31] obtained the equilibrium shapes of sessile drops over incompressible, thick linear elastic substrates by minimizing elastic and capillary free energies. They identify suitable length scales that determine the transitions in the contact angle that occur upon changing the substrate from rigid to soft.

Jerison *et al.*[21] measured the displacement fields in a silicone gel deformed due to a sessile water droplet using confocal microscopy and compared the results with the linear elasticity theory that included finite thickness, as well as surface tension of the substrate. The theory presented in the preceding work was later extended to droplets of finite size.[29] Style *et al.*[23] also considered other liquid droplets and reported that the local deformation near the contact line was universal and was independent of the droplet size and substrate thickness.

Hui and Jagota[32] analyzed the local deformation close to the contact line of an elastic half-space and identified a dimensionless parameter that governs the transition from a surface tension-dominated regime to an elasticity-dominated regime. Bostwick *et al.*[33] used dual integral equations to obtain elastic deformations of a soft substrate due to a partially wetting liquid for different contact line models.

Limat[30] obtained analytical expressions for deformation induced by straight contact lines on linear elastic solids having non-zero solid surface tension. Dervaux and Limat[34] extended the latter analysis to obtain solutions for rivulets resting on substrates. While the previous two studies were restricted to the case of linear elasticity and identical solid surface tensions over dry and wet parts of the solid, De Pascalis *et al.*[56] incorporated material and geometric non-linearities, as well as different solid surface tensions. Bardall *et al.*[57] generalized the analysis to include partial wetting, gravity, and a tangential contact line force. They found that it is important to include a horizontal traction boundary condition in order to avoid strain singularity due to inclusion of the tangential contact line force.

While the literature discussed so far mostly modelled substrates as thick elastic solids, the wetting of liquid droplets on slender elastic objects (thin plates) has also been considered.[8,13,14,58,59] Recently, Neukirch *et al.*[60] obtained equilibrium solutions to drops on elastic beams using a variational approach. This work was extended[61] to include the extension

a)Author to whom correspondence should be addressed: vnair@iitk.ac.in

of the beam. Hui and Jagota[62] considered a pendant drop hanging underneath a neo-Hookean membrane in plain strain. They report that the contact angle is not a material property and that it depends on the elasticity and geometry. They ignored gravity and the global deformation of the membrane. Schulman and Dalnoki-Veress[26] conducted experiments on micro-droplets deforming thin, free-standing films made of an elastomer and glass and found that the contact angle measured as a function of the tension in the film is described by the Neumann construction. More recently Davidovitch and Vella[35] reported that the effect of liquid drops on thin elastic sheets may be significant, in which the local stresses may be much larger than the pre-tension in the uniformly stretched dry sheet.

In this article, we obtain equilibrium shapes of sessile and pendant drops placed on elastic membranes in two-dimensions. A reason to investigate drops on membranes as opposed to thicker solids is the hope that the increased deformation observed in membranes would make such systems more accessible to experiments.[26,58,63] The use of a lower-dimensional structure like the membrane also serves to avoid mathematical issues associated with the stress singularities at the contact line, which are relevant for elastic continua. The novel features of this work are as follows. We include the effects of gravity and allow for the large deformation of the membrane under the action of capillary forces and fluid pressure. The constitutive response of the membrane is taken to be linear elastic. In contrast to the majority of the literature that focuses on the contact line geometry, we are interested here in the global properties of the system, i.e., the apparent contact angle and contact size and their variation with the volume of the drop for different membrane tensions and drop apex curvatures. Furthermore, the model presented here places no restrictions on the angle made by the drop with the membrane, which should be contrasted with previous studies that assumed that the contact angle with the undeformed substrate was 90° (neutrally wet). Our analysis reveals that the apparent contact angle is a function of the structure's geometry and is not simply a material property. Thus, even if we were to keep the membrane's material the same but change, say, its extent, the contact angle would change.

The outline of the article is as follows. In Sec. II, the mathematical model is formulated and the governing equations and boundary conditions are described. The equations obtained are solved in Sec. III. The results obtained are discussed in Sec. IV, followed by the conclusions.

II. MATHEMATICAL FORMULATION

In order to model the drop-membrane system, we place the origin O of the coordinate system at the apex of the drop and orient it such that the $\bar{y}$ axis is the line of symmetry. Figure 1 represents such a system schematically. Because we are concerned with a two-dimensional system, the drop is a two-dimensional liquid with no variations in the $\bar{z}$ direction and the membrane is in plane strain with all the deformations and forces being in the $\bar{x}-\bar{y}$ plane. Quantities with an overbar denote dimensional quantities.

The drop has a pressure $\bar{p}_l$ and a uniform density ρ_l, while the surrounding air has a pressure $\bar{p}_a$ and a uniform density ρ_a. It is assumed that the drop is much more dense than the surrounding air, i.e., $\rho_l \gg \rho_a$. The drop-air interfacial tension, denoted by γ, is uniform. The shape of the drop-air interface is given by $\bar{y} = \bar{h}(\bar{x})$. The position of the triple point, where the three phases liquid, solid, and air meet, is $(\bar{a}, \bar{h}(\bar{a}))$. The acceleration due to gravity is g.

A membrane is an elastic continuum that does not transmit or resist bending moments.[64] In its current configuration, the arc length of the membrane measured in the $\bar{x}-\bar{y}$ plane is $2(\bar{l}_1+\bar{l}_2)$, while the tension in the membrane as a function of the arc-length is $\bar{T}(\bar{x})$. In the undeformed (original) configuration, the membrane has length $2\bar{l}_0$ and uniform tension $\bar{T}_0$. It is assumed that both $\bar{T}_0$ and $\bar{T}(\bar{x})$ are much greater than the weight of the membrane. We note that in the present formulation, $\bar{T}(\bar{x})$ is taken to be the sum of mechanical tension in the membrane and surface tensions arising from the interactions of the membrane with both liquid and air. This allows us to analyze the system in a more general context, where we do not assume *a priori* that the solid-liquid and solid-air tensions are the same, an assumption most commonly made in the literature.[31,32,34] The profile of the membrane in the wet and dry parts, as shown in Fig. 1, is given by $\bar{y} = \bar{\eta}_1(\bar{x})$ and $\bar{y} = \bar{\eta}_2(\bar{x})$, respectively.

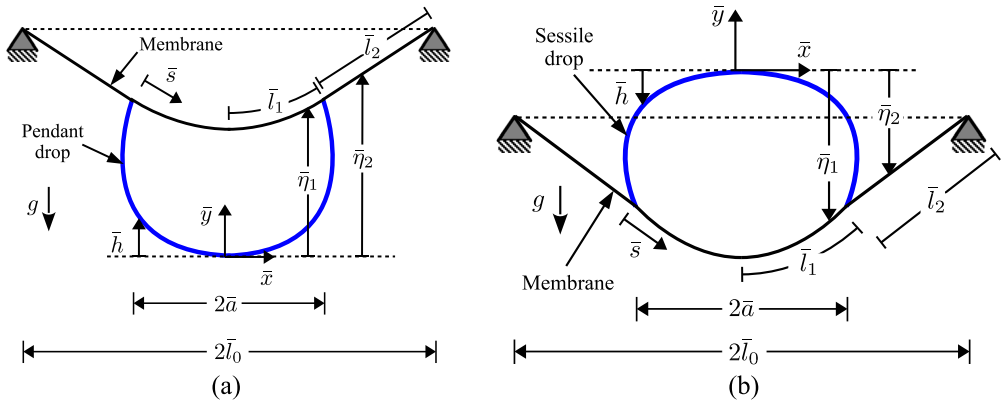

FIG. 1. Schematic of a two-dimensional (a) sessile and (b) pendant drop placed on a thin elastic membrane in plane strain. The coordinate system is placed at the apex of the drop as shown. The part of the membrane in (not in) contact with the drop is called the wet (dry) part of the membrane. The total length of the wet part is $2\bar{l}_1$, and that of the dry part is $2\bar{l}_2$. The total contact size is $2\bar{a}$. The undeformed membrane has a length $2\bar{l}_0$ and is represented by dotted lines.

A. Governing equations

Because of the spatial symmetry of the system, the domain of analysis is restricted to $0 \le \bar{x} \le \bar{l}_0$. This domain is further divided into the wet region, $0 \le \bar{x} \le \bar{a}$, and the dry region, $\bar{a} \le \bar{x} \le \bar{l}_0$, with $\bar{x} = \bar{a}$ being the position of the triple point.

The shape of the drop in equilibrium is governed by the Young-Laplace equation. For sessile and pendant drops, the Young-Laplace equation leads to

$$\frac{j\dfrac{\mathrm{d}^2\bar{h}}{\mathrm{d}\bar{x}^2}}{\left\{1+\left(\dfrac{\mathrm{d}\bar{h}}{\mathrm{d}\bar{x}}\right)^2\right\}^{3/2}} = \frac{\rho_l g\bar{h}}{\gamma} - \frac{1}{\bar{b}}, \tag{1}$$

where $j = 1$ for sessile drops and $j = -1$ for pendant drops. The above equation is the Bashforth-Adams equation adapted to two dimensions. The derivation is provided in Appendix A. The boundary conditions are

$$\bar{h} = 0 \tag{2a}$$

and

$$\frac{\mathrm{d}\bar{h}}{\mathrm{d}\bar{x}} = 0, \quad \text{at } \bar{x} = 0. \tag{2b}$$

The wet part of the membrane has tension $\bar{T}_1(\bar{x})$. The equation governing the profile of a geometrically non-linear membrane is[66]

$$j\bar{T}_1\frac{\dfrac{\mathrm{d}^2\bar{\eta}_1}{\mathrm{d}\bar{x}^2}}{\left\{1+\left(\dfrac{\mathrm{d}\bar{\eta}_1}{\mathrm{d}\bar{x}}\right)^2\right\}^{3/2}} - \left(\frac{\gamma}{\bar{b}} - \rho_l g\bar{\eta}_1\right) = 0, \tag{3}$$

which follows from balancing membrane tension and fluid pressure; see Appendix A for a derivation. The boundary conditions are

$$\frac{\mathrm{d}\bar{\eta}_1}{\mathrm{d}\bar{x}} = 0 \text{ at } \bar{x} = 0 \tag{4a}$$

and

$$\bar{\eta}_1 = \bar{h} \text{ at } \bar{x} = \bar{a}. \tag{4b}$$

In the present formulation, the volume of the drop is not a constraint imposed on the system; instead, it is calculated after obtaining the profiles of the drop and the membrane.

The dry part of the membrane has a tension $\bar{T}_2(\bar{x})$. Because this part of the membrane is free of loading, the governing equation for the membrane (3) simplifies to

$$\bar{T}_2\frac{\mathrm{d}^2\bar{\eta}_2}{\mathrm{d}\bar{x}^2} = 0. \tag{5}$$

The boundary conditions are

$$\bar{\eta}_2 = \bar{h} \text{ at } \bar{x} = \bar{a} \tag{6a}$$

and

$$\frac{\mathrm{d}\bar{\eta}_2}{\mathrm{d}\bar{x}} = \tan\,\phi \text{ at } \bar{x} = \bar{a}^+, \tag{6b}$$

where ϕ is the angle made by the dry membrane with the horizontal at the triple point and $\bar{x} = \bar{a}^+$ indicates the approach toward the triple point from the dry side.

The forces acting at the triple point $\bar{x} = \bar{a}$ are shown in Fig. 2. The force balance along the $\bar{x}$ and $\bar{y}$ directions is, respectively,

$$\bar{T}_2\cos\,\phi - \gamma\cos\,\psi - \bar{T}_1\cos\,\xi = 0 \tag{7a}$$

and

$$\bar{T}_2\sin\,\phi + j\gamma\sin\,\psi - \bar{T}_1\sin\,\xi = 0. \tag{7b}$$

The above is the appropriate generalization of Neumann's triangle[67] to the current system.

B. Non-dimensionalization

We first non-dimensionalize the governing equations for the drop. We use the capillary length $\lambda = \sqrt{\dfrac{\gamma}{\rho_l g}}$ to non-dimensionalize the variables $\bar{x}$ and $\bar{h}$, i.e., we set

$$\frac{\bar{x}}{\lambda} = x \text{ and } \frac{\bar{h}}{\lambda} = h. \tag{8}$$

Thus, the non-dimensional versions of (1) and (2) are, respectively,

$$\frac{\dfrac{\mathrm{d}^2h}{\mathrm{d}x^2}}{\left\{1+\left(\dfrac{\mathrm{d}h}{\mathrm{d}x}\right)^2\right\}^{3/2}} - j(h-\beta) = 0 \tag{9}$$

and

$$h = 0 \tag{10a}$$

and

$$\frac{\mathrm{d}h}{\mathrm{d}x} = 0 \text{ at } x = 0, \tag{10b}$$

where

$$\beta := \frac{\lambda}{\bar{b}} =: \frac{1}{b} \tag{11}$$

is the non-dimensional curvature at the apex of the drop.

We now non-dimensionalize the governing equations for the membrane. We use half the undeformed length of the membrane $\bar{l}_0$ to non-dimensionalize the variables $\bar{x}$, $\bar{\eta}_1$,

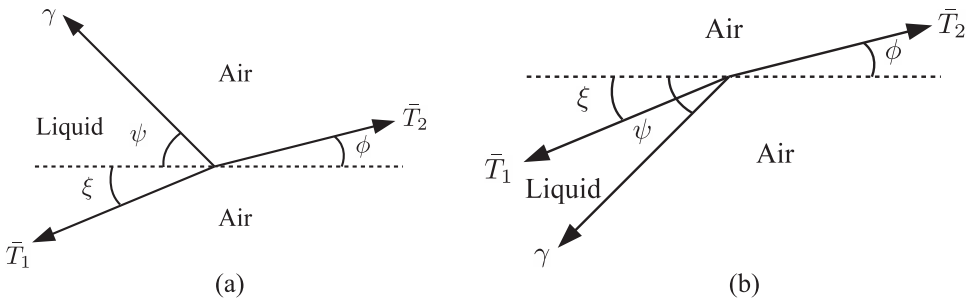

FIG. 2. Forces acting at the triple point of (a) sessile and (b) pendant drops on elastic membranes. We consider $\bar{T}_1$ and $\bar{T}_2$ to be the sum of mechanical tension in the membrane, and membrane-liquid and membrane-air surface tensions.

and $\bar{\eta}_2$ (denoted by a tilde) and surface tension γ to non-dimensionalize $\bar{T}_1$ and $\bar{T}_2$, i.e., we set

$$\frac{\bar{x}}{\bar{l}_0} = \widetilde{x}\,, \ \frac{\bar{\eta}_1}{\bar{l}_0} = \widetilde{\eta}_1\,, \ \frac{\bar{\eta}_2}{\bar{l}_0} = \widetilde{\eta}_2\,, \ \frac{\bar{T}_1}{\gamma} = \widetilde{T}_1, \ \text{ and } \ \frac{\bar{T}_2}{\gamma} = \widetilde{T}_2. \tag{12}$$

Thus, (3) and (4) are non-dimensionalized to obtain, respectively,

$$\frac{\dfrac{\mathrm{d}^2\widetilde{\eta}_1}{\mathrm{d}\widetilde{x}^2}}{\left\{1+\left(\dfrac{\mathrm{d}\widetilde{\eta}_1}{\mathrm{d}\widetilde{x}}\right)^2\right\}^{3/2}} - j\frac{c}{\widetilde{T}_1}(\beta - c\widetilde{\eta}_1) = 0 \tag{13}$$

and

$$\frac{\mathrm{d}\widetilde{\eta}_1}{\mathrm{d}\widetilde{x}} = 0 \ \text{ at } \widetilde{x} = 0 \tag{14a}$$

and

$$\widetilde{\eta}_1 = \widetilde{h} \ \text{ at } \widetilde{x} = \widetilde{a}, \tag{14b}$$

where $\widetilde{h} = \dfrac{h}{c}$ and $\widetilde{a} = \dfrac{a}{c}$ in terms of $c = \dfrac{\bar{l}_0}{\lambda}$ and $a = \dfrac{\bar{a}}{\lambda}$. Similarly, (5) and (6) are non-dimensionalized to obtain, respectively,

$$\frac{\mathrm{d}^2\widetilde{\eta}_2}{\mathrm{d}\widetilde{x}^2} = 0 \tag{15}$$

and

$$\widetilde{\eta}_2 = \widetilde{h} \ \text{ at } \widetilde{x} = \widetilde{a} \tag{16a}$$

and

$$\frac{\mathrm{d}\widetilde{\eta}_2}{\mathrm{d}\widetilde{x}} = \tan\phi \ \text{ at } \widetilde{x} = \widetilde{a}^{+}. \tag{16b}$$

Finally, (7) is non-dimensionalized to obtain

$$\widetilde{T}_2\cos\phi - \cos\psi - \widetilde{T}_1\cos\xi = 0 \tag{17a}$$

and

$$\widetilde{T}_2\sin\phi + j\sin\psi - \widetilde{T}_1\sin\xi = 0. \tag{17b}$$

We note that we have followed different non-dimensionalizations for the drop and the membrane. Thus, some quantities are scaled in two ways, e.g., the contact size $\bar{a}$ is scaled as both a and $\widetilde{a}$.

III. SOLUTION

For a given non-dimensional drop apex curvature β and contact size a, the governing equation (9) with boundary conditions (10) is solved numerically to obtain the profile of the drop. We note that the function $h(x)$, in general, is not a single valued function of x. In order to obtain shapes such as those shown in Fig. 1, we integrate (9) till the slope becomes infinite. The governing equation is then rewritten in terms of $x(h)$ and is integrated. The resulting solution is then appended to the solution obtained from (9). With the profile of the drop known, we obtain the angle ψ made by the drop with the x axis at the triple point; see Fig. 2. Next, for the same drop apex curvature β, contact size $\widetilde{a}$, and a choice of wet membrane tension $\widetilde{T}_1$, the governing equation (13) with boundary conditions (14) is solved numerically to obtain the profile of the wet membrane. With the profile of the wet membrane known for the selected $\widetilde{T}_1$, we obtain the angle ξ made by the membrane with the x axis at the triple point; see Fig. 2. Because our solution procedure calculates the drop volume *a posteriori*, the surface profile of the drop from the apex to the triple point is independent of the membrane's deformation. We choose $c = 10$, and we have verified that the results for lower values of c are found to be qualitatively similar (see footnote on p. 8964 in Ref. 62).

For the given drop apex curvature β, contact size $\widetilde{a}$, and wet membrane tension $\widetilde{T}_1$, once we know ψ and ξ, we solve (17) to obtain the dry membrane tension

$$\widetilde{T}_2 = \sqrt{\widetilde{T}_1^2 + 1 + 2\widetilde{T}_1\cos\theta}, \tag{18}$$

where $\theta = \psi + j\xi$ is the *apparent contact angle*, and the angle ϕ made by the dry membrane with the horizontal is

$$\phi = \xi - j\arccos\left(\frac{\widetilde{T}_1^2 + \widetilde{T}_2^2 - 1}{2\widetilde{T}_1\widetilde{T}_2}\right). \tag{19}$$

Turning to the dry part of the membrane, we solve (15) with boundary conditions (16) to obtain

$$\widetilde{\eta}_2 = \tan\phi(\widetilde{x} - \widetilde{a}) + \widetilde{h}(\widetilde{a}). \tag{20}$$

Once the profiles of the drop and the membrane are obtained, we rescale the membrane results to be consistent with that of the drop, i.e., we set

$$c\widetilde{x} = x\,, \ c\widetilde{\eta}_1 = \eta_1, \ \text{ and } \ c\widetilde{\eta}_2 = \eta_2.$$

Similarly, we note that the wet and dry membrane tensions are the same,

$$\widetilde{T}_1 = T_1 \ \text{ and } \ \widetilde{T}_2 = T_2.$$

Finally we calculate the drop's non-dimensional volume from

$$V = \int_{-a}^{a}\{h(x) - \eta_1(x)\}\,\mathrm{d}x. \tag{21}$$

We first quickly note the validations that we performed to benchmark our numerical procedure. We matched the surface profiles of the drops between the apex and the triple point with the appropriate two-dimensional results of Bashforth and Adams.[65] Our computations of the membrane's deformation were validated by matching with analytical results that may be obtained when deformations are small and when the pressure loading is uniformly spread over the entire length of the membrane.

We now present our results. We will investigate equilibria of the drop-membrane system for sessile and pendant drops, while varying the non-dimensional drop apex curvature β and the non-dimensional drop volume V but keeping the non-dimensional tension T_1 in the wet part of the membrane constant. There are two important things to note in this context. First, β may vary because λ or $\bar{b}$ changes or both. If we imagine that the liquid is taken to be the same, then λ is fixed, and different β correspond to drops of the *same* liquid that have *different* apex curvatures $1/\bar{b}$; cf. (11). In this article, we will consider the equilibrium shapes of a given fluid (same λ). Second, if the tension in the wet part of the deformed membrane is kept constant, then the pre-tension T_0 may vary. This may cause theoretical predictions to contradict intuition that is often predicated upon systems in which the membrane, and hence the pre-tension, is kept fixed, while the fluid's amount or type is varied. We will discuss this more in Sec. IV.

Our results for the system's global geometry are shown in Figs. 3–5. For a given fluid with a given non-dimensional

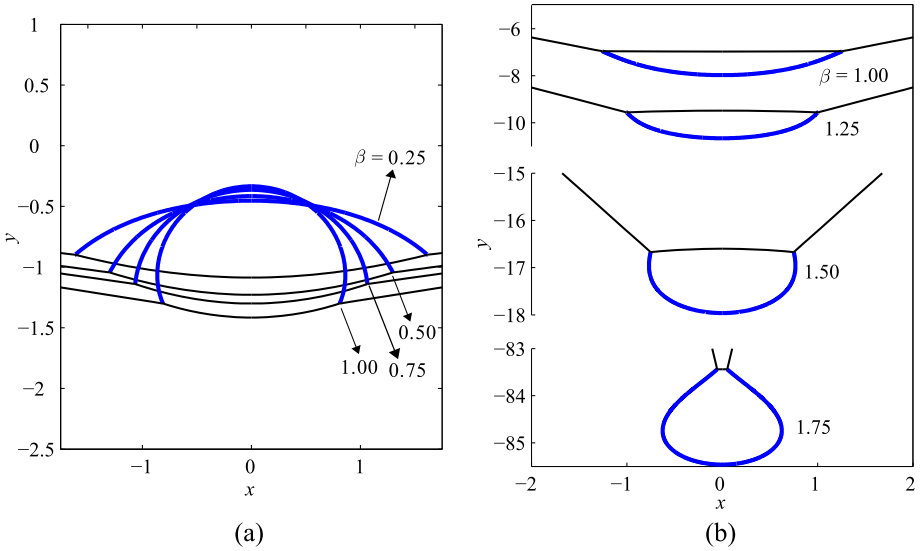

FIG. 3. Profiles of (a) sessile and (b) pendant drops on geometrically nonlinear elastic membranes for various non-dimensional drop apex curvatures β but the same non-dimensional volume V and wet membrane tension T_1. In each case, the dry part of the membrane extends up linearly to meet the end support. In (b), the ordinate is split to accommodate a solution for different β in the same plot. (a) $V = 1.5$, $T_1 = 6$. (b) $V = 1.75$, $T_1 = 0.6$.

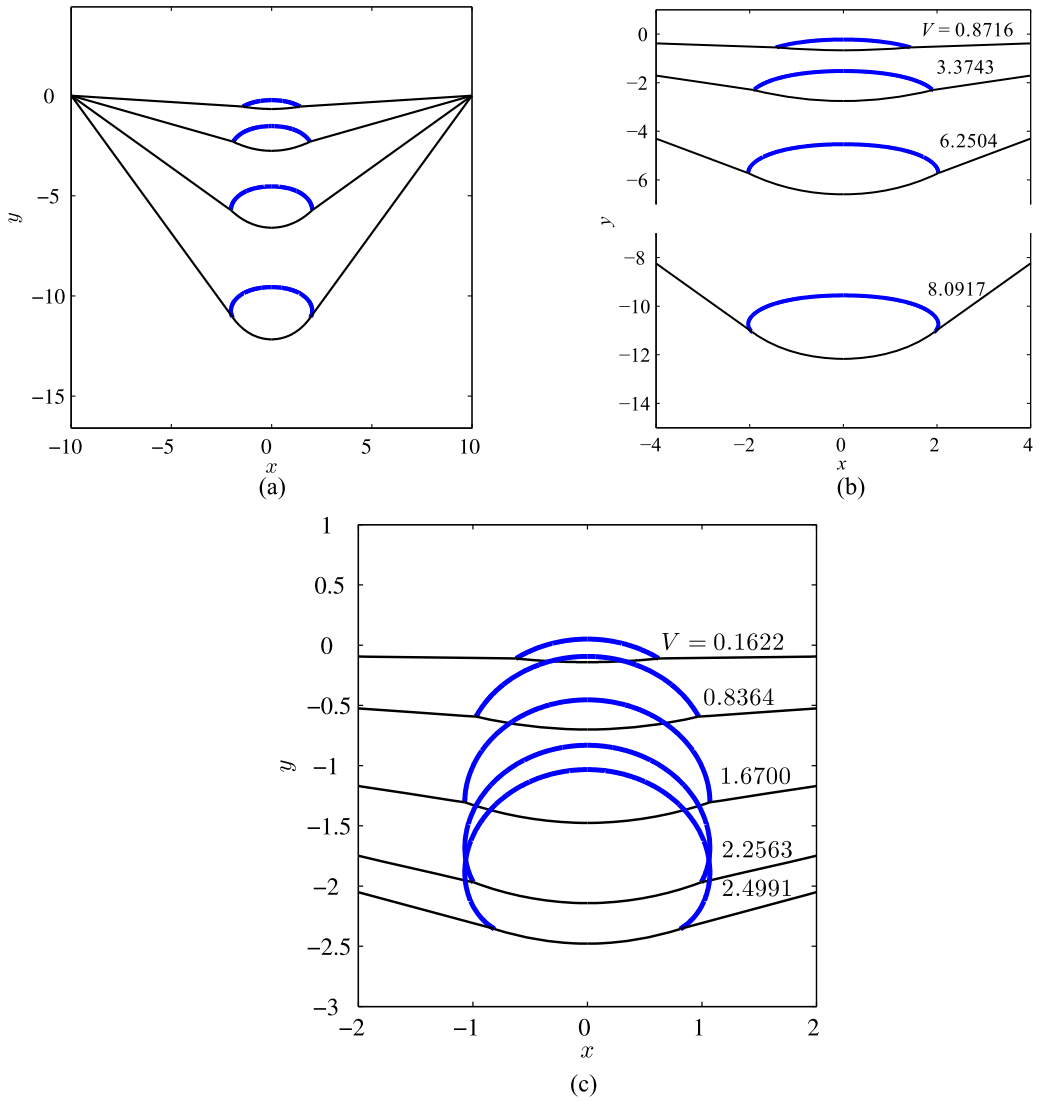

FIG. 4. Profiles of sessile drops on membranes for increasing drop volumes V. (a) Global and (b) local picture of the drop with the drop apex curvature $\beta = 0.25$. (c) Local picture of the drop with the drop apex curvature $\beta = 0.75$. The wet membrane tension $T_1 = 6$ in each case. The ordinate in (c) is split to accommodate a solution for different V in the same plot. In each case, the dry part of the membrane extends up linearly to meet the end support.

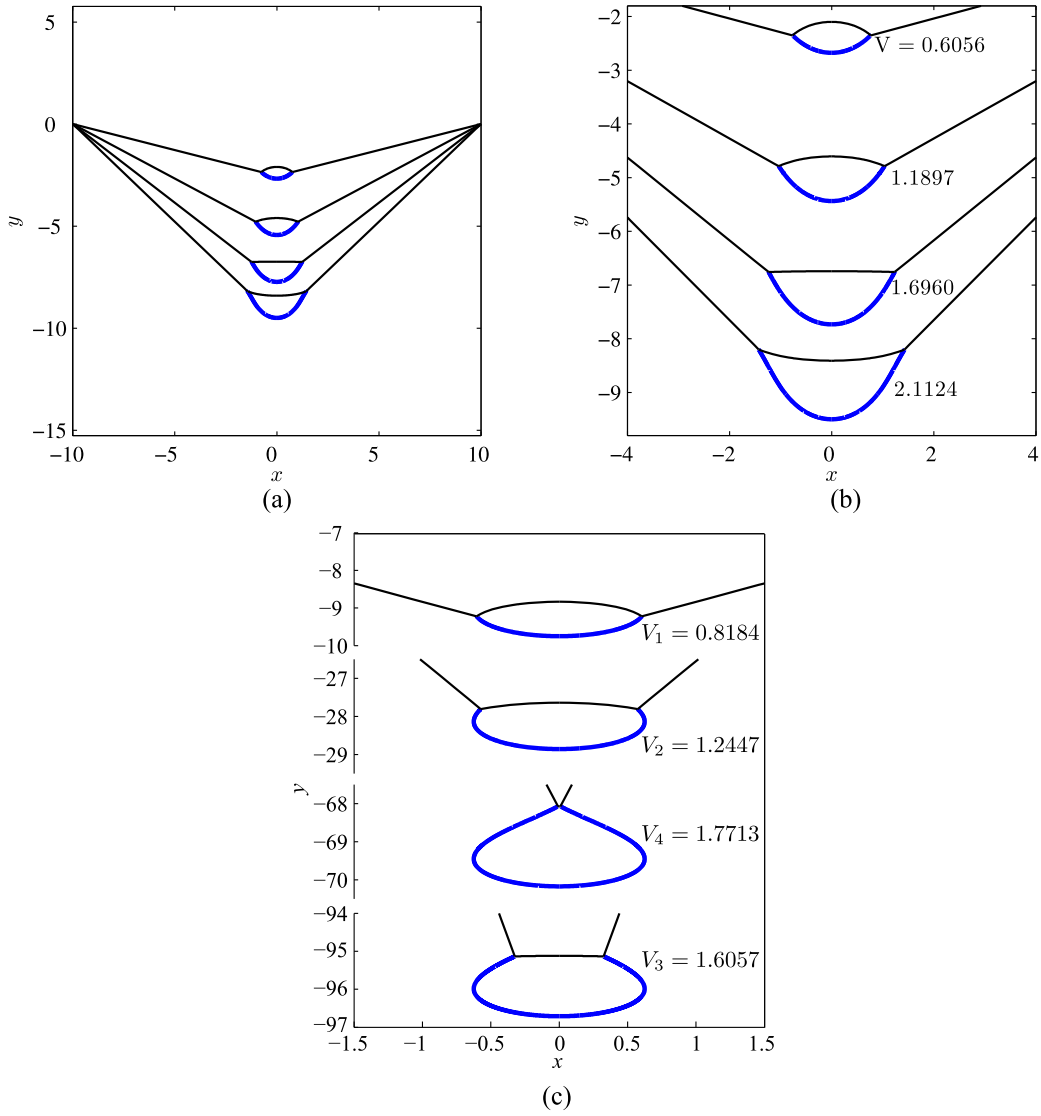

FIG. 5. Profiles of pendant drops on membranes for increasing drop volumes V. (a) Global and (b) local pictures of the drop with the drop apex curvature $\beta = 1.00$. (c) Local picture of the drop with the drop apex curvature $\beta = 1.75$. The wet membrane tension $T_1 = 0.6$ in each case. The ordinate in (c) is split to accommodate a solution for different V in the same plot. In each case, the dry part of the membrane extends up linearly to meet the end support.

volume V, Fig. 3 shows the profiles of sessile and pendant drops on membranes for different drop apex curvatures β but the same wet membrane tension T_1. Now comparing drops with different β may be considered to comparing different drop-membrane interactions. As is known, sessile drops on rigid substrates become shorter and wider when β decreases, while an increase in β results in drops taking more spherical shapes.[68] Thus, for a given fluid, a lower/higher β indicates a greater/lesser energetically favorable interaction between the drop and the membrane. Analogously, we see in Fig. 3 that as β increases, the drops take shapes that are more spherical. We also observe that when the non-dimensional apex curvature β reduces, the contact size a lowers and, even though the volume (hence the weight) of the drops are the same, the membrane's deformation increases.

Figure 4 shows the profile of sessile drops for increasing non-dimensional volumes V at fixed choices of β. As may be seen from Fig. 4, the angle ξ made by the membrane at the triple point may be large in some cases, thereby highlighting the importance of including geometric non-linearities in the description of the membrane's deformation.

Similarly, Fig. 5 shows the profile of pendant drops for increasing non-dimensional volumes V, again keeping β fixed. For small to moderately large volumes, the membrane deforms by forming an upward bulge. At larger volumes, however, the membrane is observed to sag. The upward bulging of the membrane in the axisymmetric case has been reported experimentally[24] and predicted by theory.[62] It is to be noted that in Fig. 5(b), the increase in the volume follows the order: $V_1 < V_2 < V_3 < V_4$; this, somewhat counter-intuitive prediction, is explained later when we discuss Fig. 8(b). Furthermore, for $\beta = 1.00$ in Fig. 5(b), the drop profiles are convex for small to moderately large volumes but become concave close to the contact point at larger volumes. The drop profiles for $\beta = 1.75$ in Fig. 5(b), however, remain convex even at large volumes. This suggests that when $\beta = 1.00$, the pressure difference $p_l - p_a$ changes sign at some height h^*. Because the pressure difference is directly proportional to the curvature at a

point on the interface (Young-Laplace relation), the change in sign of the pressure difference from positive to negative indicates a change in sign of the curvature at that point. This point will be revisited in Sec. IV when we discuss apparent contact angles. Finally, we again note that the angle ξ made by the membrane at the triple point is sometimes large, thereby highlighting the importance of including geometric non-linearities in the description of the membrane's deformation.

IV. RESULTS AND DISCUSSIONS

In Sec. III, the equilibrium shapes of sessile and pendant drops on geometrically non-linear elastic membranes were discussed. We now consider the variation with the drop volume V and drop apex curvature β of the following characteristics of the coupled drop-membrane system: apparent contact angle θ ($\psi + \xi$ for sessile drops and $\psi - \xi$ for pendant drops), contact size a, dry membrane tension T_2, slopes ϕ, ξ, and ψ at the triple point of, respectively, the dry membrane, the wet membrane, and the drop's surface; cf. Fig. 2. All results shown below are obtained by keeping the wet membrane tension T_1 fixed at an indicated value. The results corresponding to other values of T_1 show similar trends in general and thus have not been discussed. We now reiterate an important comment made earlier. The wet membrane tension T_1 can be related to the pre-tension T_0 in the membrane before the drop is placed; cf. Appendix B. It is possible that T_0 be different even though T_1 is the same. This may, sometimes, as for $\beta = 1.75$ in Fig. 8(b) below, cause results to run contrary to our expectations that are, typically, predicated upon T_0 being constant. All such instances will be highlighted.

Figure 6 shows the variation of the contact size a with the drop volume V for any choice of β. The contact size of sessile drops in Fig. 6(a) is observed to grow initially with the volume and then reduce. This non-monotonic behavior is different from that of drops on rigid substrates, where the contact size always grows with the volume. This may be explained as follows: We take a constant β to correspond to the same liquid (i.e., same capillary length λ) with the same apex curvature (same $\bar{b}$) and, thus, the same membrane. In such cases, as the drop's volume grows, so does its weight, which deforms the membrane more. After a point, further increase in the drop's volume is accommodated by the membrane's increased sag (see Fig. 4), which leads to a lowering in the contact size a. We recover the rigid-limit by having large tension T_1 (see Appendix C).

The pendant drops in Fig. 6(b) display two different behaviors. For smaller β, the contact size grows monotonically, but for larger β, a grows non-monotonically. This contrasting behavior may be linked to whether or not the curvature of the drop's surface changes its sign—at low β, we noticed in Fig. 5(a) that the surface became concave at large V—while at larger β in Fig. 5(b), the surface remained convex even at large V. We define β^* to be the drop apex curvature at which the contact size in Fig. 6(b) ceases to display a monotonic behavior. Typically $1.25 < \beta^* < 1.50$ for $T_1 = 0.6$.

Finally, for a given V, the contact size decreases with an increase in β for both sessile and pendant drops. As discussed in the context of Fig. 3, comparing drops with different β may be considered to comparing drops with the same capillary length λ (same drop) but different dimensional apex curvatures ($1/\bar{b}$) (different drop-membrane interactions). Then a lower β corresponds to a more energetically favorable droplet-membrane interaction, and vice versa. Thus, at lower β, the drops spread more and have higher contact areas, which decreases as β increases; see also Fig. 3.

Figure 7 shows changes in the slope of the drop's surface with the horizontal at the triple point with the drop volume V. This angle is constant for drops on rigid substrates and corresponds to the equilibrium contact angle. From Fig. 7(a), we observe that the sessile drop's slope ψ increases monotonically with the drop's volume V when the drop apex curvature β is kept fixed. This behavior may be understood in conjunction with Fig. 6(a) where we noticed that the increase in the drop's volume was accommodated by the enhanced sag of the membrane. Because of this, the contact size first grew and then reduced, and this is reflected in the drop's slope ψ when it switches from acute (<90°) to obtuse (>90°). From Fig. 7(b), we observe that a pendant drop's slope ψ varies non-monotonically with the drop's volume V when the drop apex curvature β is kept fixed.

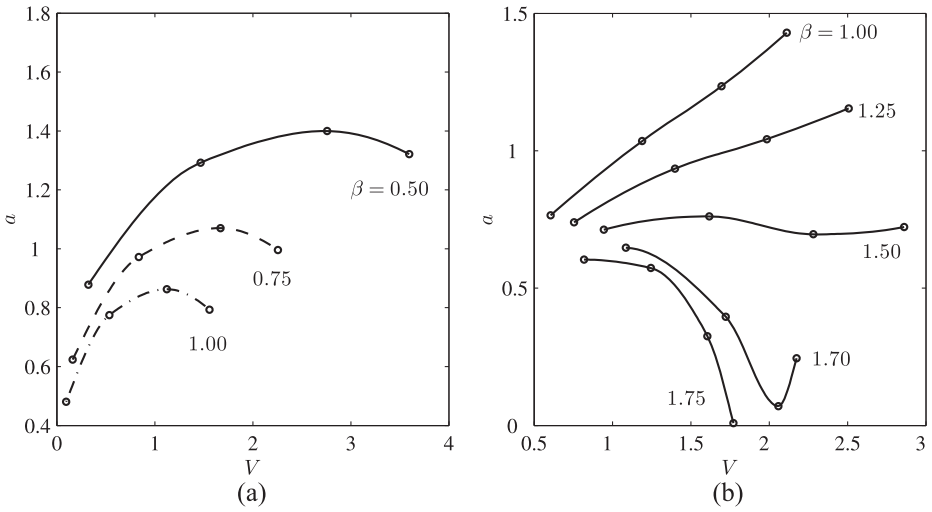

FIG. 6. Variation of the contact size a with the volume V of (a) sessile and (b) pendant drops. We investigate several drop apex curvatures β as indicated next to the associated curves. (a) $T_1 = 6$ and (b) $T_1 = 0.6$.

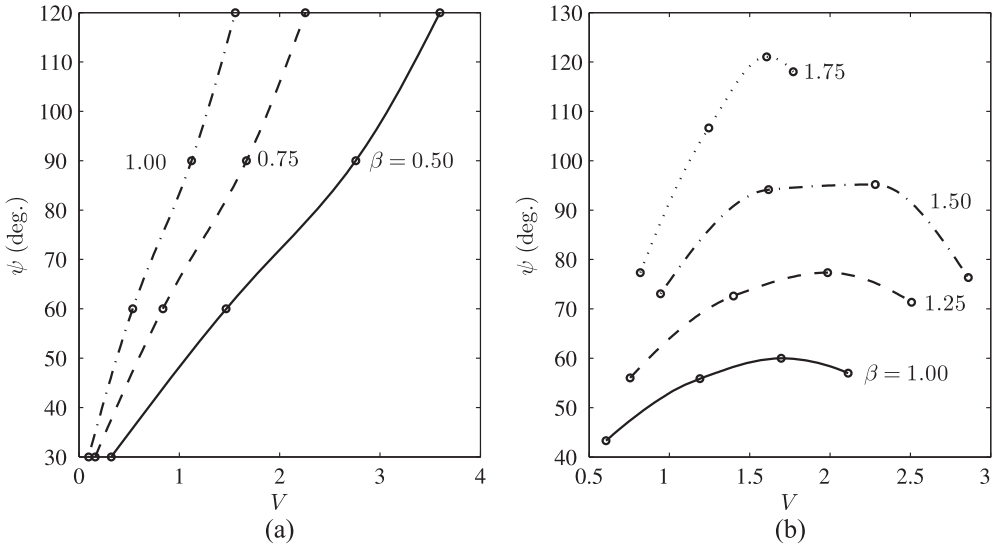

FIG. 7. Variation of the slope ψ made by (a) sessile and (b) pendant drops at the triple point with the volume V of the drop. We investigate several drop apex curvatures β as indicated next to their associated curves. (a) $T_1 = 6$. (b) $T_1 = 0.6$.

Next, for a given V, ψ increases with β for both sessile and pendant drops in Fig. 7. This, as was noted above, is because a larger β may be taken to correspond to a lesser energetically favorable drop-membrane interaction, which causes the liquid surface to enter the triple point at larger ψ; see Fig. 3.

Figure 8 shows the variation of the slope ϕ made by the dry part of the membrane at the triple point with the volume V of the drop. It is noted that enlarging the volume of both sessile and pendant drops (for $\beta^* < \beta$) augments ϕ for all drop apex curvatures β. An increment in the volume makes the weight of the drop larger, thereby depressing the membrane more. Furthermore, for a given volume, an increase in the drop apex curvature β elevates ϕ. This is because as β increases for a given V, the contact size decreases (Fig. 6). Thus the weight of the drop acts up on a narrower part, causing the membrane to deform more.

The decrease in ϕ eventually with V for pendant drops with $\beta^* > \beta$ in Fig. 8(b) is due to the difference in pre-tension T_0 values in the membrane; see Appendix B. We recall from the first paragraph of this section that T_0 may be different if T_1 is kept constant. Indeed, for $V_1 = 0.8184$, $T_0 = 0.5716$; $V_2 = 1.2447$, $T_0 = 0.5998$; $V_3 = 1.6057$, $T_0 = 0.6004$; and $V_4 = 1.7713$, $T_0 = 0.6010$. We observe that as V increases, so does the pre-tension, and an initially stiffer membrane has to deflect less to support a greater volume. This explains both the decrease in ϕ in Fig. 8(b) and the observations of Fig. 5(b), wherein the drop with the volume V_4 deflected the membrane less than the drop with the volume V_3 even though $V_4 > V_3$. However, in Fig. 13 of Appendix B, we show the monotonic increase in membrane deformation with the volume V for constant pre-tension T_0.

Figure 9 shows the variation of the slope ξ made by the wet part of the membrane at the triple point with the volume V of the drop. From Fig. 9(a), we observe that for sessile drops, ξ increases with the drop volume for any choice of the drop apex curvature β. This is because when the drop's volume is larger, so is its weight acting upon the membrane, causing it to deform more. For pendant drops, we note from Fig. 9(b) that negative ξ correspond to the *bulging* up of

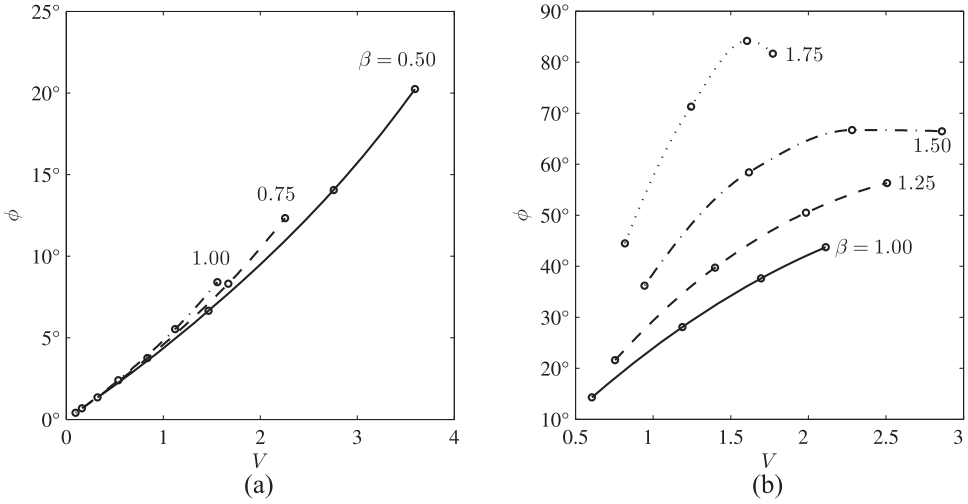

FIG. 8. Variation of the slope ϕ made by the dry part of the membrane at the triple point with the volume V of (a) sessile and (b) pendant drops. We investigate several drop apex curvatures β as indicated next to their associated curves. (a) $T_1 = 6$. (b) $T_1 = 0.6$.

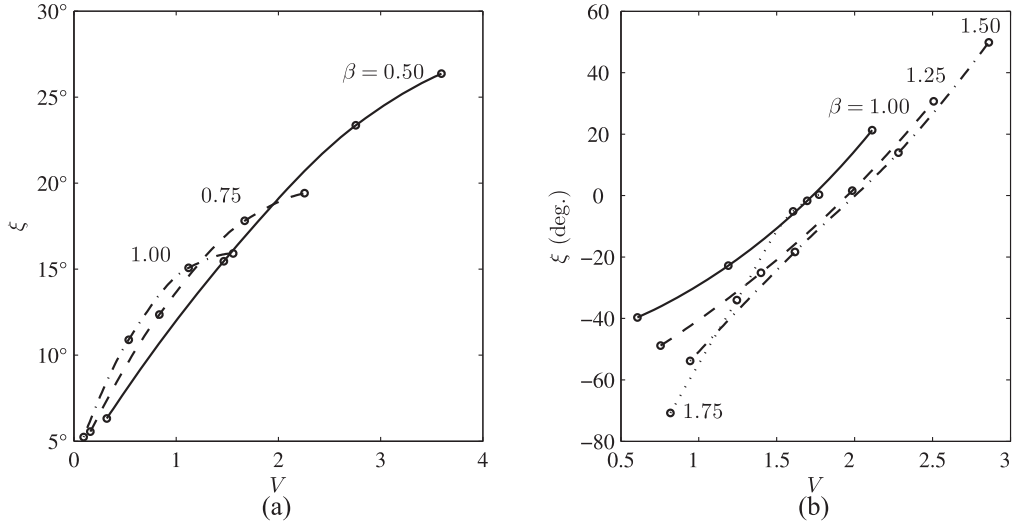

FIG. 9. Variation of the slope ξ made by the wet part of the membrane at the triple point with the volume V of (a) sessile and (b) pendant drops. We investigate several drop apex curvatures β as indicated next to their associated curves. (a) $T_1 = 6$. (b) $T_1 = 0.6$.

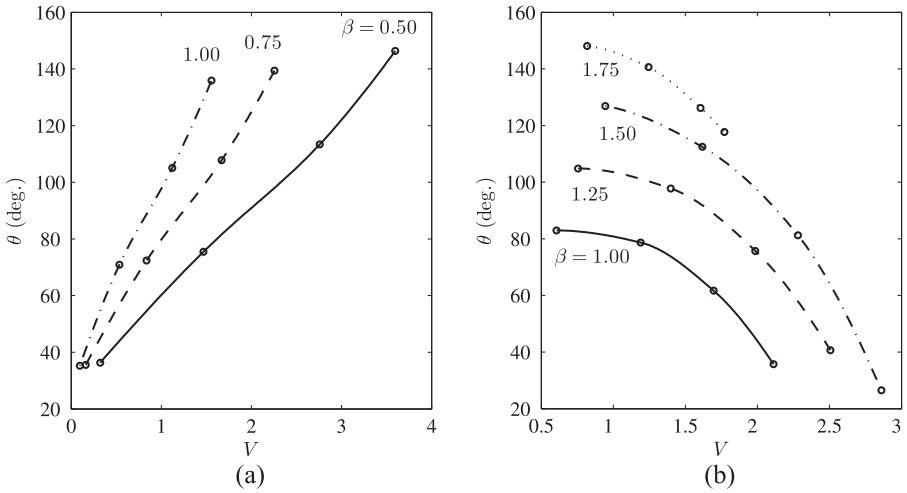

FIG. 10. Variation of the apparent contact angle θ with the volume V of (a) sessile and (b) pendant drops. We investigate several drop apex curvatures β as indicated next to their associated curves. (a) $T_1 = 6$. (b) $T_1 = 0.6$.

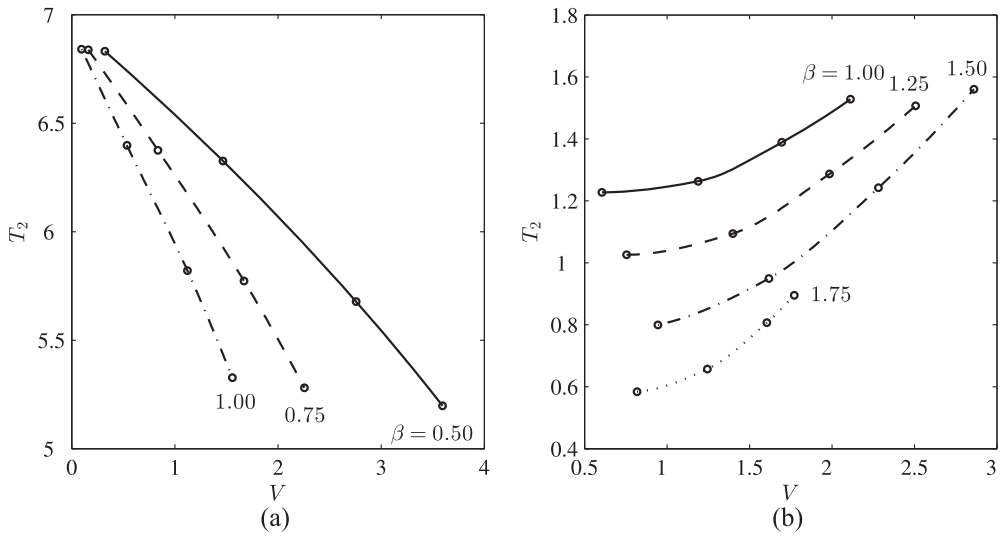

FIG. 11. Variation of the dry membrane tension T_2 with the volume V of (a) sessile and (b) pendant drops. We investigate several drop apex curvatures β as indicated next to their associated curves. (a) $T_1 = 6$. (b) $T_1 = 0.6$.

the membrane, as seen in Fig. 5. For higher volumes, however, the bulge gradually reduces and the membrane starts sagging, as may be observed in Fig. 5. There is thus a volume for which the wet membrane remains flat even though there is a pendant drop below. In this configuration, the dry part is not flat as the force balance at the triple point must hold.

Figure 10 shows the variation with the drop volume V of the apparent contact angle θ ($\psi + \xi$ for sessile drops and $\psi - \xi$ for pendant drops) made by drops at the triple point. From Fig. 10(a), we observe that for sessile drops, θ increases with the drop volume for any choice of the drop apex curvature β. This is explained by noting that an increase in the drop volume augments the weight of the drop, if we consider, as we do, that a fixed β corresponds to the drops of the same liquid with the same dimensional apex curvature $(1/\bar{b})$. This results in an increase in the slope ψ as well as ξ, as may be seen from Figs. 7(a) and 9(a). The opposite, however, is the case for pendant drops where, in Fig. 10(b), we find that θ lowers with the elevation in the drop volume. Furthermore, for a given V, θ increases with β for both sessile and pendant drops. This is because, as noted before, the increase in the drop apex curvature reduces the contact area, causing the weight of the drop to act upon a narrower part of the membrane, leading to a greater deformation.

Figure 11 shows the variation of the dry membrane tension T_2 with the volume V of the drop. From (18), we note that for a given wet membrane tension T_1, T_2 is a function of only the apparent contact angle λ. Thus, we observe from Fig. 11(a) that for sessile drops, T_2 strictly decreases as V grows for all drop apex curvatures β. At lower V, $T_2 > T_1$, while at larger V, the converse holds. However, for pendant drops, we observe from Fig. 11(a) that T_2 increases with V for all drop apex curvatures β and $T_2 > T_1$ for all V. Furthermore, for a given V, T_2 lowers when β is augmented for both sessile and pendant drops.

V. CONCLUSION

In this work, we have obtained equilibrium solutions of drops on geometrically non-linear elastic membranes in two-dimensions. Both sessile and pendant drops were considered. The profiles obtained correspond to different combinations of drop-membrane interactions, contact size, and membrane tension. Subsequently, the properties of the system were analyzed.

It was found that for sessile drops, the apparent contact angle increased with the drop volume for all drop apex curvatures. However, in the case of pendant drops, the apparent contact angle decreased with the drop volume. Also, for a given drop volume, the apparent contact angle increased with the drop apex curvature for both sessile and pendant drops. Apart from being a material property, it was noted that the apparent contact angle depends on the system's geometry as well. It was also noted that for sessile drops, the contact size varied non-monotonically with the drop volume for all drop apex curvatures. For pendant drops, however, the contact size increased with the volume for drop apex curvatures below a critical value.

As a sequel to this work, the equilibrium shapes of axisymmetric drops placed on geometrically non-linear circular elastic membranes will be analyzed both theoretically and experimentally.

APPENDIX A: DERIVATION OF THE GOVERNING EQUATIONS

We first derive the governing equations for a two-dimensional drop placed on a solid surface. The derivation provided here follows that of Bashforth and Adams.[65] At a point on the interface between the two fluids, the Young-Laplace equation is

$$\bar{p}_a - \bar{p}_l = -\gamma \nabla \cdot \hat{\boldsymbol{n}},$$

where $\hat{\boldsymbol{n}}$ is the unit normal from the drop toward the surrounding fluid and $\nabla \cdot \hat{\boldsymbol{n}}$ is the curvature, both measured at the point under consideration. Now, $\bar{p}_a - \bar{p}_l = \bar{p}_a - (\bar{p}_{l0} - \rho_l g \bar{h}) = (\bar{p}_{a0} - \bar{p}_{l0}) + \rho_l g \bar{h} = -\frac{\gamma}{\bar{b}} + \rho_l g \bar{h}$, where $\bar{p}_{l0}$ and $\bar{b}$ are, respectively, the fluid pressure and the radius of the curvature at the drop's apex. The last equality follows from the application of the Young-Laplace equation at the drop's apex. The curvature at the point under consideration is

$$\nabla \cdot \hat{\boldsymbol{n}} = \frac{-j \dfrac{\mathrm{d}^2 \bar{h}}{\mathrm{d}\bar{x}^2}}{\left\{1 + \left(\dfrac{\mathrm{d}\bar{h}}{\mathrm{d}\bar{x}}\right)^2\right\}^{3/2}},$$

where $j = \pm 1$ for sessile/pendant drops. Thus, the Young-Laplace equation reduces to

$$\frac{j \dfrac{\mathrm{d}^2 \bar{h}}{\mathrm{d}\bar{x}^2}}{\left\{1 + \left(\dfrac{\mathrm{d}\bar{h}}{\mathrm{d}\bar{x}}\right)^2\right\}^{3/2}} - \left(\frac{\rho_l g \bar{h}}{\gamma} - \frac{1}{\bar{b}}\right) = 0,$$

which governs the equilibrium shape of a two-dimensional drop.

We now derive the governing equation for a geometrically non-linear membrane in plane strain. At a position s along the length of the membrane, an element of length Δs is considered. The forces acting on this element are shown in Fig. 12. Tensions $\bar{T}_1(s)$ and $\bar{T}_1(s + \Delta s)$ act along the tangential directions, at positions s and $s + \Delta s$, respectively. The resultant of the distributed forces, $f(s + \Delta s^*)$, is assumed to act along the normal direction at the position $s + \Delta s^*$, where $\Delta s^* \leq \Delta s$. The tangential and normal unit vectors at any position s are $\hat{\boldsymbol{t}}(s)$ and $\hat{\boldsymbol{n}}(s)$, respectively. For both sessile and pendant drops, the normal $\hat{\boldsymbol{n}}(s)$ always points away from the drop and toward the surrounding air. The angles made by $\hat{\boldsymbol{t}}(s)$ with the $\bar{x}$ axis is $\theta(s)$. In order to calculate $f(s + \Delta s^*)$, we note that at a point on the membrane, the total traction exerted by the drop and air is $(\bar{p}_l - \bar{p}_a)\boldsymbol{I} \cdot \hat{\boldsymbol{n}}(s + \Delta s^*)$, where $\boldsymbol{I}$ is the identity tensor. The distributed force intensity vector is, thus, $\boldsymbol{f}(s + \Delta s^*) = (\bar{p}_l - \bar{p}_a)\Delta s\, \hat{\boldsymbol{n}}(s + \Delta s^*)$.

The force balance along the direction $\hat{\boldsymbol{t}}(s)$ is

$$-j\bar{T}_1(s + \Delta s)\cos\{\theta(s + \Delta s) - \theta(s)\} + j\bar{T}_1(s) - (\bar{p}_l - \bar{p}_a)\sin\{\theta(s + \Delta s) - \theta(s)\}\Delta s = 0,$$

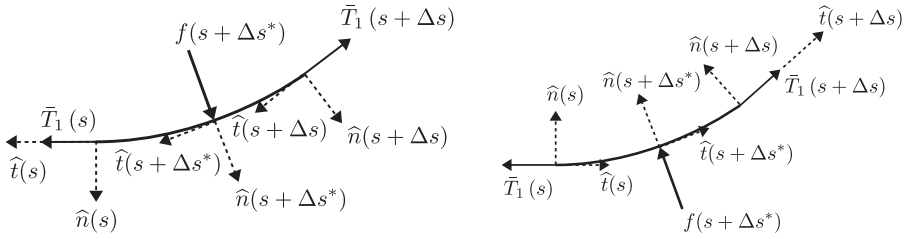

FIG. 12. Free body diagram of an element of the membrane in plane strain when a (a) sessile drop and (b) pendant drop are placed.

and that along the direction $\hat{\boldsymbol{n}}(s)$ is

$$-j\bar{T}_1(s+\Delta s)\sin\{\theta(s+\Delta s)-\theta(s)\} + (\bar{p}_l-\bar{p}_a)\cos\{\theta(s+\Delta s)-\theta(s)\}\Delta s = 0,$$

where, as noted above, $j = 1$ is for sessile drops and $j = -1$ is for pendant drops. As $\Delta s \to 0$, the tangential force balance reduces to $\mathrm{d}\bar{T}_1/\mathrm{d}s = 0$ so that $\bar{T}_1 = C$, a constant. The normal force balance, with $\Delta s \to 0$, now results in

$$-j\bar{T}_1\frac{\mathrm{d}\theta(s)}{\mathrm{d}s} + (\bar{p}_l-\bar{p}_a) = 0.$$

We note that

$$\frac{\mathrm{d}\theta(s)}{\mathrm{d}s} = \frac{\dfrac{\mathrm{d}^2\bar{\eta}_1}{\mathrm{d}\bar{x}^2}}{\left\{1+\left(\dfrac{\mathrm{d}\bar{\eta}_1}{\mathrm{d}\bar{x}}\right)^2\right\}^{3/2}}$$

and

$$\bar{p}_l-\bar{p}_a = \frac{\gamma}{\bar{b}} - \rho_l g\bar{\eta}_1.$$

Thus, we obtain

$$j\bar{T}_1\frac{\dfrac{\mathrm{d}^2\bar{\eta}_1}{\mathrm{d}\bar{x}^2}}{\left\{1+\left(\dfrac{\mathrm{d}\bar{\eta}_1}{\mathrm{d}\bar{x}}\right)^2\right\}^{3/2}} - \left(\frac{\gamma}{\bar{b}} - \rho_l g\bar{\eta}_1\right) = 0$$

as the governing equation for a geometrically non-linear membrane in plane strain.

APPENDIX B: PRE-TENSION IN THE MEMBRANE

In its undeformed state, the membrane has a length $2\bar{l}_0$ and a uniform tension $\bar{T}_0$. The undeformed shape is depicted by dotted lines in Fig. 1. A symmetrically placed drop around the midpoint of the membrane deforms it, and the system assumes the equilibrium shape shown by solid lines in Fig. 1.

In its deformed state, the membrane has uniform tensions $\bar{T}_1$ and $\bar{T}_2$ in the wet and dry parts of the membrane, respectively. The wet and dry parts of the membrane have total lengths $2l_1$ and $2l_2$, respectively. Due to spatial symmetry, we focus our analysis to the region $0 \le \bar{x} \le \bar{l}_0$. The material point where tension is discontinuous, i.e., the triple point, has coordinates $(\bar{s}^*, 0)$ in the undeformed state.

We now obtain a relationship between non-dimensional tensions T_0 and T_1. The change in the length of the wet part of the membrane is

$$\bar{l}_1 - \bar{s}^* = \frac{\bar{T}_1-\bar{T}_0}{AE}\bar{s}^*,$$

and that of the dry part of the membrane is

$$\bar{l}_2 - (\bar{l}_0-\bar{s}^*) = \frac{\bar{T}_2-\bar{T}_0}{AE}(\bar{l}_0-\bar{s}^*),$$

where E is the membrane's Young's modulus and A is its cross-sectional area. In our two dimensional analysis, A is the membrane thickness. In non-dimensional terms, the above equations reduce to

$$l_1 - s^* = \frac{\gamma}{E}\frac{T_1-T_0}{A}s^*$$

and

$$l_2 - (l_0-s^*) = \frac{\gamma}{E}\frac{T_2-T_0}{A}(l_0-s^*),$$

where the ratio $\dfrac{\gamma}{E}$ is the elastocapillary length.[4] We can solve the above two equations to obtain s^* and T_0. For example, for $\beta = 1.75$ in Fig. 5(c), we obtain with $\dfrac{\gamma}{E} = 1e{-}03$ and $A = 1e-06$ the following pre-tensions: for $V_1 = 0.8184$, $T_0 = 0.5716$; $V_2 = 1.2447$, $T_0 = 0.5998$; $V_3 = 1.6057$, $T_0 = 0.6004$; and $V_4 = 1.7713$, $T_0 = 0.6010$.

It was observed in Fig. 5(b) that the drop with the volume V_4 deflected the membrane less than the drop with the volume V_3 even though $V_4 > V_3$. The figure had a constant wet membrane tension $T_1 = 6$. In Fig. 13, we have, for the same $\beta = 1.75$, pendant drop profiles for different wet membrane tensions but for the same pre-tension $T_0 = 0.85$. We observe that the increasing volume

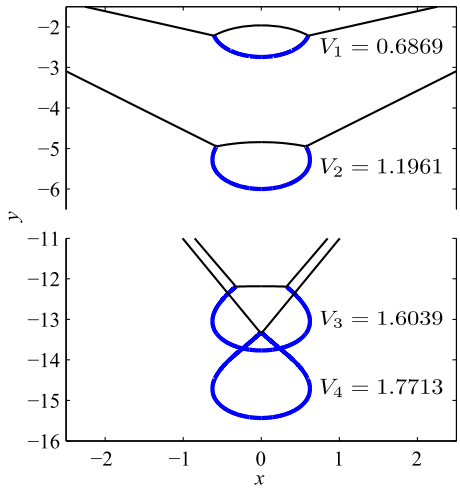

FIG. 13. Profiles of pendant drops on membranes for increasing drop volumes V. Local picture of the drop with the drop apex curvature $\beta = 1.75$. The membrane pre-tension is $T_0 = 0.85$ in each case. The ordinate is split to accommodate a solution for different V in the same plot. In each case, the dry part of the membrane extends up linearly to meet the end support.

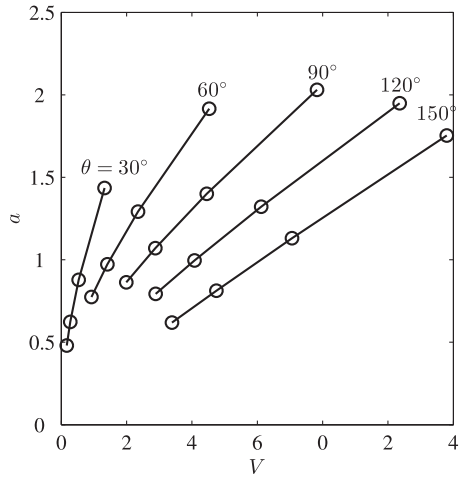

FIG. 14. Variation of the contact radius a with the volume V for large pre-tension T_0. The open circles denote the data points corresponding to the case of rigid substrates.

V results in a monotonic increase in the deformation of the membrane.

APPENDIX C: VARIATION OF CONTACT RADIUS WITH VOLUME IN THE RIGID LIMIT

Figure 14 shows that in the limit of large pre-tension T_0, our results approach those obtained for a truly rigid substrate.

APPENDIX D: AN ALTERNATE LENGTH SCALE

For the sake of completeness, Fig. 15 shows the profiles of sessile drops on membranes obtained by keeping the drop apex radius of the curvature as the length scale for non-dimensionalizing both the drop and the membrane. However, there is a caveat in adopting this length scale. This procedure does not, however, capture the phenomenon that the contact angle is not just a material property but indeed a function of the geometrical and material properties of the membrane-fluid system.

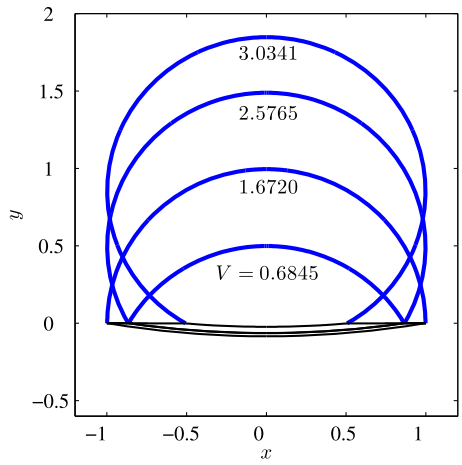

FIG. 15. Profiles of sessile drops on membranes for increasing drop volumes V using the alternate length scale. The non-dimensional parameter here corresponds to $\beta = 10$. The wet membrane tension $T_1 = 6$ in each case.

[1]B. Roman and J. Bico, "Elasto-capillarity: Deforming an elastic structure with a liquid droplet," J. Phys.: Condens. Matter **22**, 493101 (2010).
[2]B. Andreotti, O. Bäumchen, F. Boulogne, K. E. Daniels, E. R. Dufresne, H. Perrin, T. Salez, J. H. Snoeijer, and R. W. Style, "Solid capillarity: When and how does surface tension deform soft solids?," Soft Matter **12**, 2993–2996 (2016).
[3]B. Andreotti and J. H. Snoeijer, "Soft wetting and the shuttleworth effect, at the crossroads between thermodynamics and mechanics," Europhys. Lett. **113**, 66001 (2016).
[4]R. W. Style, A. Jagota, C.-Y. Hui, and E. R. Dufresne, "Elastocapillarity: Surface tension and the mechanics of soft solids," Annu. Rev. Condens. Matter Phys. **8**, 99 (2017).
[5]J. Bico, É. Reyssat, and B. Roman, "Elastocapillarity: When surface tension deforms elastic solids," Annu. Rev. Fluid Mech. **50**, 629 (2018).
[6]G. R. Lester, "Contact angles of liquids at deformable solid surfaces," J. Colloid Sci. **16**, 315–326 (1961).
[7]A. I. Rusanov, "Theory of wetting of elastically deformed bodies. 1. Deformation with a finite contact-angle," Colloid J. USSR **37**, 614–622 (1975).
[8]M. A. Fortes, "Deformation of solid surfaces due to capillary forces," J. Colloid Interface Sci. **100**, 17–26 (1984).
[9]S. H. Yuk and M. S. Jhon, "Contact angles on deformable solids," J. Colloid Interface Sci. **110**, 252–257 (1986).
[10]M. E. R. Shanahan and P.-G. De Gennes, "Equilibrium of the triple line solid/liquid/fluid of a sessile drop," in *Adhesion 11*, edited by K. W. Allen (Elsevier Applied Science, 1987), pp. 71–81.
[11]M. E. R. Shanahan, "The influence of solid micro-deformation on contact angle equilibrium," J. Phys. D: Appl. Phys. **20**, 945 (1987).
[12]J. J. Métois, "Elastic straining of a thin graphite layer by a liquid droplet or a non-epitaxed Pb crystallite," Surf. Sci. **241**, 279–288 (1991).
[13]R. Kern and P. Müller, "Deformation of an elastic thin solid induced by a liquid droplet," Surf. Sci. **264**, 467–494 (1992).
[14]J. Olives, "Capillarity and elasticity. The example of the thin plate," J. Phys.: Condens. Matter **5**, 2081 (1993).
[15]A. Carré, J.-C. Gastel, and M. E. R. Shanahan, "Viscoelastic effects in the spreading of liquids," Nature **379**, 432 (1996).
[16]C. W. Extrand and Y. Kumagai, "Contact angles and hysteresis on soft surfaces," J. Colloid Interface Sci. **184**, 191–200 (1996).
[17]J. Olives, "A combined capillarity and elasticity problem for a thin plate," SIAM J. Appl. Math. **56**, 480–493 (1996).
[18]L. R. White, "The contact angle on an elastic substrate. 1. The role of disjoining pressure in the surface mechanics," J. Colloid Interface Sci. **258**, 82–96 (2003).
[19]R. Pericet-Cámara, A. Best, H.-J. Butt, and E. Bonaccurso, "Effect of capillary pressure and surface tension on the deformation of elastic surfaces by sessile liquid microdrops: An experimental investigation," Langmuir **24**, 10565–10568 (2008).
[20]R. Pericet-Cámara, G. K. Auernhammer, K. Koynov, S. Lorenzoni, R. Raiteri, and E. Bonaccurso, "Solid-supported thin elastomer films deformed by microdrops," Soft Matter **5**, 3611–3617 (2009).
[21]E. R. Jerison, Y. Xu, L. A. Wilen, and E. R. Dufresne, "Deformation of an elastic substrate by a three-phase contact line," Phys. Rev. Lett. **106**, 186103 (2011).
[22]A. Marchand, S. Das, J. H. Snoeijer, and B. Andreotti, "Capillary pressure and contact line force on a soft solid," Phys. Rev. Lett. **108**, 094301 (2012).
[23]R. W. Style, R. Boltyanskiy, Y. Che, J. S. Wettlaufer, L. A. Wilen, and E. R. Dufresne, "Universal deformation of soft substrates near a contact line and the direct measurement of solid surface stresses," Phys. Rev. Lett. **110**, 066103 (2013).
[24]N. Nadermann, C.-Y. Hui, and A. Jagota, "Solid surface tension measured by a liquid drop under a solid film," Proc. Natl. Acad. Sci. U. S. A. **110**, 10541–10545 (2013).
[25]S. J. Park, B. M. Weon, J. S. Lee, J. Lee, J. Kim, and J. H. Je, "Visualization of asymmetric wetting ridges on soft solids with x-ray microscopy," Nat. Commun. **5**, 4369 (2014).
[26]R. D. Schulman and K. Dalnoki-Veress, "Liquid droplets on a highly deformable membrane," Phys. Rev. Lett. **115**, 206101 (2015).
[27]Q. Xu, K. E. Jensen, R. Boltyanskiy, R. Sarfati, R. W. Style, and E. R. Dufresne, "Direct measurement of strain-dependent solid surface stress," Nat. Commun. **8**, 555 (2017).
[28]R. D. Schulman, M. Trejo, T. Salez, E. Raphaël, and K. Dalnoki-Veress, "Surface energy of strained amorphous solids," Nat. Commun. **9**, 982 (2018).

[29]R. W. Style and E. R. Dufresne, "Static wetting on deformable substrates, from liquids to soft solids," Soft Matter **8**, 7177–7184 (2012).
[30]L. Limat, "Straight contact lines on a soft, incompressible solid," Eur. Phys. J. E **35**, 134 (2012).
[31]L. A. Lubbers, J. H. Weijs, L. Botto, S. Das, B. Andreotti, and J. H. Snoeijer, "Drops on soft solids: Free energy and double transition of contact angles," J. Fluid Mech. **747**, R1 (2014).
[32]C.-Y. Hui and A. Jagota, "Deformation near a liquid contact line on an elastic substrate," Proc. R. Soc. A **470**, 20140085 (2014).
[33]J. B. Bostwick, M. Shearer, and K. E. Daniels, "Elastocapillary deformations on partially-wetting substrates: Rival contact-line models," Soft Matter **10**, 7361–7369 (2014).
[34]J. Dervaux and L. Limat, "Contact lines on soft solids with uniform surface tension: Analytical solutions and double transition for increasing deformability," Proc. R. Soc. A **471**, 20140813 (2015).
[35]B. Davidovitch and D. Vella, "Partial wetting of thin solid sheets under tension," Soft Matter **14**, 4913 (2018).
[36]J. H. Snoeijer, E. Rolley, and B. Andreotti, "Paradox of contact angle selection on stretched soft solids," Phys. Rev. Lett. **121**, 068003 (2018); preprint arXiv:1803.04428 (2018).
[37]M. Sokuler, G. K. Auernhammer, M. Roth, C. Liu, E. Bonacurrso, and H.-J. Butt, "The softer the better: Fast condensation on soft surfaces," Langmuir **26**, 1544–1547 (2009).
[38]K. E. Jensen, R. Sarfati, R. W. Style, R. Boltyanskiy, A. Chakrabarti, M. K. Chaudhury, and E. R. Dufresne, "Wetting and phase separation in soft adhesion," Proc. Natl. Acad. Sci. U. S. A. **112**, 14490–14494 (2015).
[39]R. W. Style, C. Hyland, R. Boltyanskiy, J. S. Wettlaufer, and E. R. Dufresne, "Surface tension and contact with soft elastic solids," Nat. Commun. **4**, 2728 (2013).
[40]R. W. Style, Y. Che, S. J. Park, B. M. Weon, J. H. Je, C. Hyland, G. K. German, M. P. Power, L. A. Wilen, J. S. Wettlaufer *et al.*, "Patterning droplets with durotaxis," Proc. Natl. Acad. Sci. U. S. A. **110**, 12541–12544 (2013).
[41]S. Karpitschka, A. Pandey, L. A. Lubbers, J. H. Weijs, L. Botto, S. Das, B. Andreotti, and J. H. Snoeijer, "Liquid drops attract or repel by the inverted Cheerios effect," Proc. Natl. Acad. Sci. U. S. A. **113**, 7403–7407 (2016).
[42]J. Huang, M. Juszkiewicz, W. H. De Jeu, E. Cerda, T. Emrick, N. Menon, and T. P. Russell, "Capillary wrinkling of floating thin polymer films," Science **317**, 650–653 (2007).
[43]D. Vella, M. Adda-Bedia, and E. Cerda, "Capillary wrinkling of elastic membranes," Soft Matter **6**, 5778–5782 (2010).
[44]B. Davidovitch, R. D. Schroll, D. Vella, M. Adda-Bedia, and E. A. Cerda, "Prototypical model for tensional wrinkling in thin sheets," Proc. Natl. Acad. Sci. U. S. A. **108**, 18227–18232 (2011).
[45]C. Py, P. Reverdy, L. Doppler, J. Bico, B. Roman, and C. N. Baroud, "Capillary origami: Spontaneous wrapping of a droplet with an elastic sheet," Phys. Rev. Lett. **98**, 156103 (2007).
[46]S. Jung, P. M. Reis, J. James, C. Clanet, and J. W. M. Bush, "Capillary origami in nature," Phys. Fluids **21**, 091110 (2009).
[47]J. W. Van Honschoten, J. W. Berenschot, T. Ondarcuhu, R. G. P. Sanders, J. Sundaram, M. Elwenspoek, and N. R. Tas, "Elastocapillary fabrication of three-dimensional microstructures," Appl. Phys. Lett. **97**, 014103 (2010).
[48]N. D. Brubaker and J. Lega, "Capillary-induced deformations of a thin elastic sheet," Philos. Trans. R. Soc., A **374**, 20150169 (2016).
[49]C. J. Howland, A. Antkowiak, J. R. Castrejón-Pita, S. D. Howison, J. M. Oliver, R. W. Style, and A. A. Castrejón-Pita, "It's harder to splash on soft solids," Phys. Rev. Lett. **117**, 184502 (2016).
[50]R. D. Schulman, R. Ledesma-Alonso, T. Salez, E. Raphaël, and K. Dalnoki-Veress, "Liquid droplets act as 'compass needles' for the stresses in a deformable membrane," Phys. Rev. Lett. **118**, 198002 (2017).
[51]S. Mondal, M. Phukan, and A. Ghatak, "Estimation of solid–liquid interfacial tension using curved surface of a soft solid," Proc. Natl. Acad. Sci. U. S. A. **112**, 12563–12568 (2015).
[52]Q. Xu, R. W. Style, and E. R. Dufresne, "Surface elastic constants of a soft solid," Soft Matter **14**, 916–920 (2018).
[53]R. W. Style and Q. Xu, "The mechanical equilibrium of soft solids with surface elasticity," Soft Matter **14**, 4569–4576 (2018); preprint arXiv:1801.07744 (2018).
[54]S. Das, A. Marchand, B. Andreotti, and J. H. Snoeijer, "Elastic deformation due to tangential capillary forces," Phys. Fluids **23**, 072006 (2011).
[55]A. Marchand, S. Das, J. H. Snoeijer, and B. Andreotti, "Contact angles on a soft solid: From Young's law to Neumann's law," Phys. Rev. Lett. **109**, 236101 (2012).
[56]R. De Pascalis, J. Dervaux, I. Ionescu, and L. Limat, "Numerical multiscale modelling of nonlinear elastowetting," Eur. J. Mech. A: Solids **71**, 151 (2018).
[57]A. Bardall, K. E. Daniels, and M. Shearer, "Deformation of an elastic substrate due to a resting sessile droplet," Eur. J. Appl. Math. **29**, 281–300 (2018).
[58]M. E. R. Shanahan, "Contact angle equilibrium on thin elastic solids," J. Adhes. **18**, 247–267 (1985).
[59]M. E. R. Shanahan, "Equilibrium of liquid drops on thin plates; plate rigidity and stability considerations," J. Adhes. **20**, 261–274 (1987).
[60]S. Neukirch, A. Antkowiak, and J.-J. Marigo, "The bending of an elastic beam by a liquid drop: A variational approach," Proc. R. Soc. A **469**, 20130066 (2013).
[61]S. Neukirch, A. Antkowiak, and J.-J. Marigo, "Soft beams: When capillarity induces axial compression," Phys. Rev. E **89**, 012401 (2014).
[62]C.-Y. Hui and A. Jagota, "Planar equilibrium shapes of a liquid drop on a membrane," Soft Matter **11**, 8960–8967 (2015).
[63]R. D. Schroll, M. Adda-Bedia, E. Cerda, J. Huang, N. Menon, T. P. Russell, K. B. Toga, D. Vella, and B. Davidovitch, "Capillary deformations of bendable films," Phys. Rev. Lett. **111**, 014301 (2013).
[64]S. P. Timoshenko and S. Woinowsky-Krieger, *Theory of Plates and Shells* (McGraw-Hill, 1959).
[65]F. Bashforth and J. C. Adams, *An Attempt to Test the Theories of Capillary Action* (University Press, 1883).
[66]S. S. Antman, *Nonlinear Problems of Elasticity* (Springer, 2005).
[67]P.-G. De Gennes, F. Brochard-Wyart, and D. Quéré, *Capillarity and Wetting Phenomena: Drops, Bubbles, Pearls, Waves* (Springer, 2004).
[68]C. Pozrikidis, *Fluid Dynamics: Theory, Computation, and Numerical Simulation* (Springer, 2016).